Topological Analysis of Ag–Ag and Ag–N Interactions in Silver Amidinate Precursor Complexes of Silver Nanoparticles

Maxime Puyo, Emilie Lebon Tailhades, Laure Vendier, Myrtil L. Kahn, Pierre Fau, Katia Fajerwerg, Christine Lepetit

Topological analysis of Ag-Ag and Ag-N interactions in silver-amidinate precursor complexes of silver nanoparticles

Maxime Puyo, Emilie Lebon, Laure Vendier, Myrtil L. Kahn, Pierre Fau*, Katia Fajerwerg*, Christine Lepetit*

LCC-CNRS, Université de Toulouse, CNRS, UPS, Toulouse, France.
E-mail: christine.lepetit@lcc-toulouse.fr, pierre.fau@lcc-toulouse.fr
katia.fajerwerg@lcc-toulouse.fr

Keywords: silver-amidinate complexes, argentophilic interaction, ELF and QTAIM topological analyses, metal-metal bond

Abstract: A series of silver-amidinate complexes is studied both experimentally and theoretically, in order to investigate the role of the precursor complex in the control of the synthesis of silver nanoparticles via an organometallic route. The replacement of the methyl substituent of the central carbon atom of the amidinate anion by a *n*-butyl group, allows for the crystallization of a tetranuclear silver-amidinate complex **3** instead of a mixture of di- and trinuclear silver-amidinate complexes **1** and **2**, as obtained with a methyl substituent. The relative stabilities and dissociation schemes of various isomeric arrangements of silver atoms in **3** are investigated at the computational DFT level of calculation, depending on the substituents of the amidinate ligand. A tetranuclear silver-amidinate complex **4**, exhibiting a diamond-like arrangement of the four silver atoms is also considered. Ag-N bonds and argentophilic Ag-Ag interactions are finely characterized using ELF and QTAIM topological analyses, and compared over the series of the related di, tri and tetranuclear silver-amidinate complexes **1**-**4**. In contrast to the Ag-N dative bonds very similar over the series, argentophilic Ag-Ag interactions of various strengths and covalence degree are characterized for complexes **1**-**4**. This gives insight into the role of the amidinate substituents on the nuclearity and intramolecular chemical bonding of the silver-amidinate precursors, required for the synthesis of dedicated AgNPs with chemically well-defined surfaces.

Introduction

Silver offers a vast panel of fascinating properties thanks to its remarkable electrical, optical, chemical, (electro)catalytic and biological features. In addition, a cohort of new and exciting physical and chemical properties emerge for Ag cores, when confined under the form of small size nanoparticles, exhibiting a high surface to volume ratio. Silver nanoparticles (AgNPs) are employed as biomedical agents, [1] they exhibit optical properties due to a strong localized surface plasmon resonance (LSPR) that can expand from the visible to the near-infrared (NIR) range. [2, 3] They find also applications in catalysis or bio-catalysis reactions. [4-6] Unpredicted properties can arise at the bottom range of the nanoscale. For example, coinage Ag atoms of AgNPs of 1-3 nm size, exhibit red or NIR photoluminescence properties. [7]

The observation of nano-sized Ag particles is almost as ancient as the colloidal gold prepared by Faraday in 1857, since it followed it by about thirty years with the seminal work of Lea. [8] Since then, the chemical synthesis of metal nanoparticles in solution or in colloidal medium, has been one of the most employed way to prepare AgNPs up to the gram scale. **[6]** However, the synthesis and characterization of small-size AgNPs in solution, remains a challenge. A huge majority of reports, describing the synthesis methods of AgNPs in various solvents, **[6, 9]** refer to the archetypal silver nitrate ($AgNO_3$) precursor. [10] Due to the required harsh reduction conditions, either by strong agents such as $NaBH_4$ [11] or by hot oleylamine (180°C), [12] the resulting AgNPs of size larger than 10 nm, exhibit a complex surface chemistry, mixing both reducing agents and surfactants.

The synthesis of AgNPs of controlled morphology and surface chemistry is therefore a hot topic. **[12]** The role of the salt or complex precursor on the nucleation and growth of AgNPs is poorly discussed in the literature, [13] and was only recently emphasized as a key feature towards the control of the AgNPs surface architecture, size and size dispersion. [14]

An attractive route for the synthesis of AgNPs, is based on the decomposition or hydrogenolysis of metalorganic precursors in organic solvents. However, very few silver precursor complexes have been proposed so far. Using triphenylphosphine silver precursors (PPh_3)Ag-X, where X is a nitrate or a chloride anion, the control of the size and purity of AgNPs could not be achieved due to the high decomposition temperature and concentration of counterions in solution. [13,15] The size of the AgNPs was reported to depend on the functional group X. Noteworthy, the released PPh_3 ligands are contributing to the stabilizing coating shell of AgNPs, as shown by IR spectroscopy. **[13]**

Metal-amidinates have been recently developed as new class of precursors of metallic NPs. Their decomposition properties are expected to be tunable, as the bridging N, N donor amidinates offer a large potential of functionalization on both the central carbon atom and nitrogen atoms. [16] Because of their high thermal stability, Cu, Al, or Ag-amidinates have been used for chemical vapor deposition or atomic layer deposition of metal or metal oxide layers.[17] Polynuclear silver-amidinate precursors are well-suited to the mild hydrogenolysis conditions towards highly controlled AgNPs. Mixtures of dinuclear and trinuclear silver-(N,N'-diisopropylacetamidinate) complexes **1** and **2** (Scheme 1), prepared in the solid state or in solution at various concentration ratio according to the Gordon's procedure, [18] have been reported to yield small-size AgNPs of narrow size distribution. [19] Furthermore, it was shown that the amidine derivatives released upon hydrogenolysis of the precursor, are contributing to the protecting outer-shell of the colloidal AgNPs. **[19]** These precursors are therefore not only the metal source, but they contain intrinsic stabilizing ligands released during the reduction process.

The replacement of the methyl substituent of the central carbon atom of the N,N'-diisopropylacetamidinate anion by a bulkier *n*-butyl group, allowed for the synthesis of the tetranuclear silver-(N-N'-diisopropyl-*n*-butylamidinate) complex **3** (Scheme 1). The hydrogenolysis of the latter yielded AgNPs included in devices for the electrochemical detection of aqueous pollutant. [20]

The X-ray diffraction characterization of **3** is described hereafter for the first time (Figure 1). Among bridged silver-amidinate complexes, very few other tetranuclear representatives are reported. The crystal structure of three complexes, among which silver-(N,N'-diphenylpropamidinate) **4**, exhibiting a diamond-like arrangement of the four silver atoms, were disclosed by Archibald *et al.*. **[16]** More recently, other tetranuclear complexes featuring similar diamond-like arrangements of the silver atoms were obtained using formamidinate[21] or 5,5-bicyclic amidinates. [22]

In order to investigate the relation between the variation of the nuclearity and the silver atoms arrangement in the **1**-**4** series, and the substituents of the amidinate ligand, Density Functional Theory (DFT) studies were performed. The stabilities and dissociation schemes of various isomeric arrangements of silver atoms in **3** and **4** were studied.

In order to gain further insight into the role of the amidinate substituents in the control of chemically well-defined AgNPs surfaces, the electronic structure of complexes **1**-**4** has been studied using quantum theory of atoms in molecules (QTAIM)[23] and electron localized function (ELF) analyses. [24] The latter topological analyses have been shown to be unique theoretical tools for chemical bonding analysis. [25] QTAIM analyses of related silver complexes have been

already reported, [26] but joint QTAIM and ELF analyses will be described hereafter for the first time, in order to finely characterize metal-ligand and metal-metal interactions and tentatively understand their role, in the various nuclearities and silver arrangement in the **1-4** series.

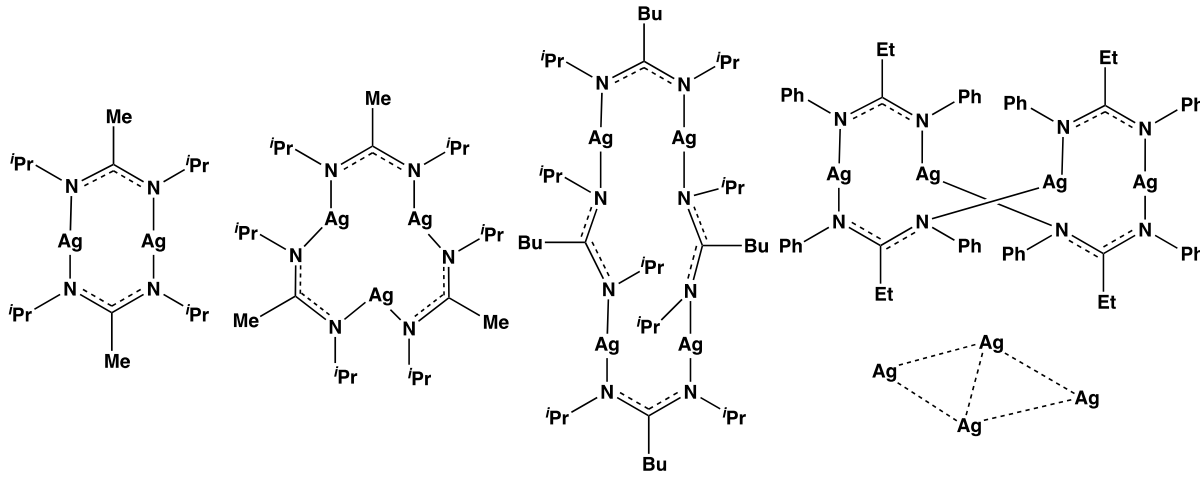

1 **2** **3** **4**

Scheme 1. Structures of the silver-amidinate complexes studied in this work

The synthesis and X-ray diffraction characterization of tetranuclear complex **3** will be first described. Gibbs free energies of various isomers of **3** and **4** and their derivatives, will be compared in order to discuss the most favorable arrangement of the four silver atoms depending on various substituents of either the central C atom (methyl (Me) or *n*-butyl (*n*-Bu)) or of the N atoms (isopropyl (^{i}Pr) or phenyl (Ph)) of the amidinate ligand. DFT calculation of dissociation energies of **3** into the related di- and trinuclear silver-amidinate complexes, depending on the substituents (Me, *n*-Bu) of the central carbon atom of the amidinate anionic ligand, will allow to investigate the role of the latter on the nuclearity of the precursor complexes. Finally, the metal-ligand and metal-metal bonding (nature and strength) in silver-amidinate complexes **1-4** will be discussed on the basis of the relevant QTAIM and ELF descriptors.

Results and discussion

*Structure of silver N-N'-diisopropyl-n-butylamidinate (**3**)*

The synthesis of **3,** adapted from the report of Lim *et al.* for silver N-N'-diisopropylacetamidinate complexes **1** and **2**, [18] and its spectroscopic characterization**,** have been reported elsewhere. [20] The first step of the synthesis, namely the reaction of an

alkyllithium with a carbodiimide affording the corresponding lithium amidinate, is followed by a metathesis with a silver halide compound to yield complex **3**. Single crystals of **3** were grown from their saturated diethylether solution, kept at -40°C for a week, to allow recrystallization. White crystals were obtained with a typical yield of 40 %.

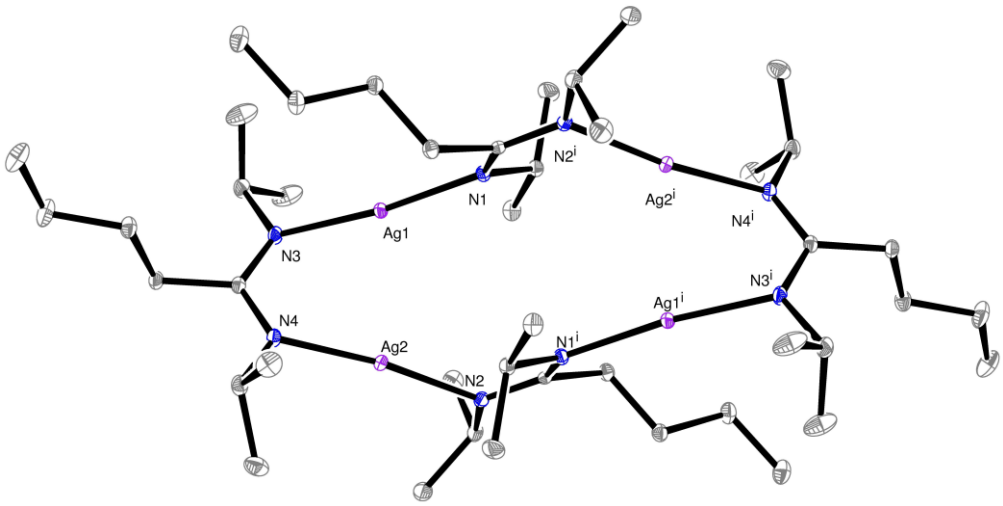

Figure 1. ORTEP diagram of tetranuclear silver-amidinate complex **3**. Thermal ellipsoids are shown at the 30% probability level. Hydrogen atoms have been omitted for clarity. The isopropyl groups are nearly equally disordered over two sites but only one site is shown here. Bond lengths (Å) and angles (°) : Ag1-N1 = 2.1062 (15), Ag1-N3 = 2.0937 (15), Ag2-N4 = 2.1117 (15), Ag2-N2 = 2.1242 (15), Ag1-Ag2 =2.8494 (2), N3-Ag1-N1 = 173.03 (6), N3-Ag1-Ag2 = 78.48 (4), N1-Ag1-Ag2 = 107.40 (4), N4-Ag2-N2 = 173.18 (6), N4-Ag2-Ag1 = 77.79 (4), N2-Ag2-Ag1 = 108.72 (4).

The solid-state characterization of **3** by single-crystal X-ray diffraction studies, yields the experimental structure of C_i symmetry shown in Figure 1. In contrast to diisopropylacetamidinate, yielding a mixture of dinuclear and trinuclear silver complexes **1** and **2** in the solid state, [18] a unique species, namely tetranuclear silver complex **3**, is obtained in the solid-state, using diisopropyl-*n*-butylamidinate. The latter complex of C_i symmetry exhibits a 16-membered ring involving the four silver atoms, connected each other by bridging μ, κ^1(N):κ^1(N')-diisopropyl-*n*-butylamidinate ligands (Figure 1). The Ag-N distances (2.10 - 2.13 Å range, mean value 2.11 Å), are close to the ones in complexes **1** and **2** (**1**: 2.11 Å, **2**: 2.09 - 2.14 Å range, mean value 2.12 Å) (Figure 1 and Table S1). The Ag-Ag distance of 2.85 Å in **3** is intermediate between the shorter value (2.65 Å) in the dinuclear complex **1** and the larger values (2.86 Å, 2.90 Å and 3.20 Å) in the trinuclear complex **2** (Table S1). These intermetallic distances, much shorter than twice the van der Waals radius of silver (i.e. 3.44 Å),[27] are indicative of argentophilic interactions.

The packing of the tetranuclear complexes in the crystal does not involve any intermolecular Ag-Ag interactions nor any intermolecular hydrogen bonds. The shorter contacts occurring between two hydrogen atoms (2.28 Å) or between one hydrogen atom and one carbon atom (2.88 Å) of the alkyl substituents of the amidinate anions, thus about the sum of their van der Waals radii, suggest the absence of intermolecular steric constraints or stabilizing weak interactions. The conformation of the 16-membered ring of **3** is therefore not influenced by weak intermolecular interactions in the crystal but rather by intramolecular ones such as hydrogen bonding.

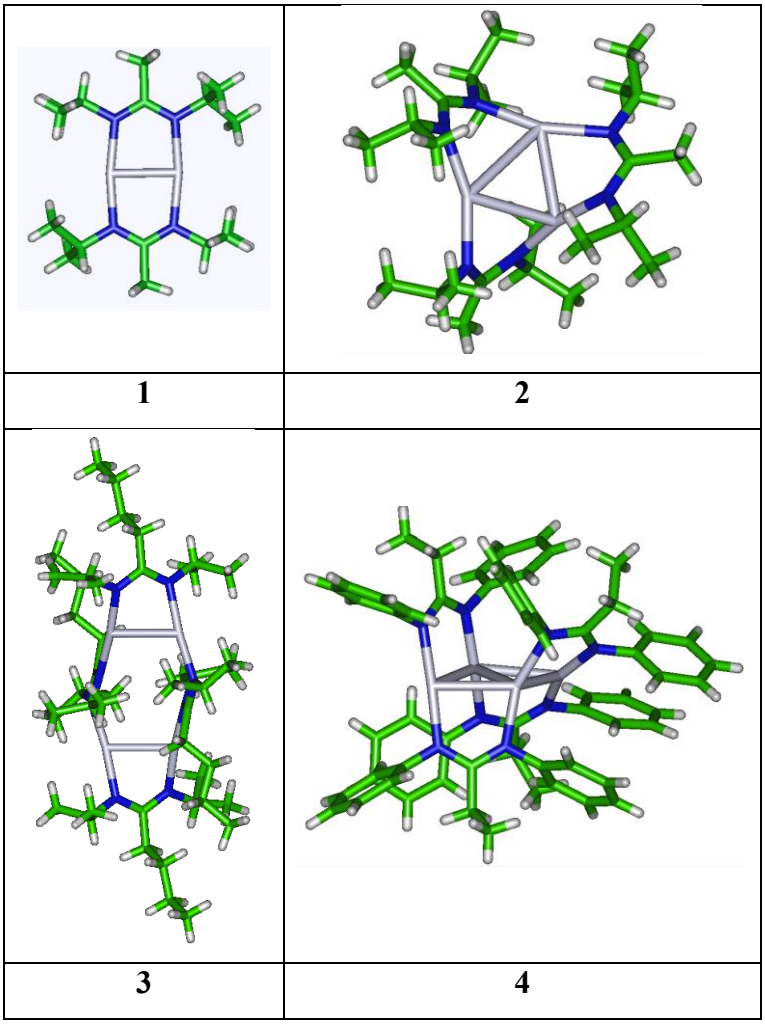

Figure 2. Experimental structures of complexes **1-4.** Silver atoms are displayed in gray, nitrogen atoms in blue, carbon atoms in green and hydrogen atoms in white colour.

To the best of our knowledge, few crystal structures of tetranuclear silver-amidinate complexes were reported in the literature: [16] (i) a structure involving a distorted diamond arrangement of the four silver atoms was disclosed by Irwin *et al.*; [28] (ii) a series of three

complexes, among which **4**, which is built from N-N'-diphenylpropamidinate, involving a planar diamond arrangement of the four silver atoms (Figure 2). [16] Complex **4** may be envisioned as the result of the folding of complex **3**, about an axis joining both central carbon atoms of the central bridging amidinates. The Ag-N distances (2.09 - 2.13 Å range, average value 2.12 Å) are almost invariant with the amidinate substituents, as they are lying in the same range as the ones of complexes **1-3** (Table S1).

In contrast to the Ag-N distances that are very similar, the Ag-Ag distances and the silver atoms arrangements are very different over the **1-4** series (Table S1). Various arrangements of four silver atoms within tetranuclear complexes have been reported. In order to investigate the most favorable one, the relative (Gibbs free) energies of four possible isomers of complex **3** were calculated in vacuum or taking into account the tetrahydrofuran (THF) solvent as a continuum (Figure 3 and Figure S1).

The geometry of isomers **4Bu** and **4Me**, in which the original diphenyl-propylamidinate ligands of **4** were respectively substituted by diisopropyl-*n*-butylamidinate and diisopropylacetamidinate ligands, were optimized at the PBE-D3/def2TZVP level of calculation. The planar diamond arrangement of the four silver atoms in **4Bu** is less stable by 4.2 kcal mol^{-1} than the one of **3** (Figure 3). On the basis of their relative Gibbs free energies, a mixture of both structures is therefore expected in solution.

Isomer **Ag4pyBu**, featuring a pyramidal arrangement of the four silver atoms, inspired from the one of a tetranuclear silver complex built with dithiobenzoate ligands, [29] was also considered (Figure 3). However, **Ag4pyBu** was found much less stable, namely 28 kcal mol^{-1} higher in energy than **3**. Finally, a twisted conformation of complex **3** was also found much higher in energy than **3** and **4Bu** (14.6 kcal mol^{-1}) (Figure 3). In the calculated structure of **Ag4pyBu**, some Ag-N and Ag-Ag distances are respectively elongated up to 2.59 Å and 2.97 Å as compared to the ones in **3** (Table S1), in order to accommodate the steric constraints of the four bridging amidinates, suggesting that the corresponding weaker dative Ag-N bonds and argentophilic interactions results in a less stable structure. The same holds for the twisted conformation of **3**.

The geometries of **3Me** and **3PhEt** were built by substitution of diisopropyl-*n*-butylamidinate ligands by diisopropylacetamidinate and diphenyl-propylamidinate ligands respectively. While the optimized structures of **3Me** and **4Me** are found quasi-degenerate in energy, but with a reversed stability order, in vacuum or in the THF solvent (Figure S1), **4** is found more stable by 13.8 kcal mol^{-1} than **3PhEt** (Figure S1). This is in agreement with the

obtention of **4** in the solid-state experimentally and illustrate that the amidinate substituent may have a strong influence on the metal center arrangement.

From the above theoretical studies, the planar diamond-like arrangement of the four silver atoms in **4Bu** appears therefore to be thermodynamically as favorable as the one observed in **3**. A mixture of both isomers may therefore be expected in solution for both the methyl or *n*-butyl substituent of the amidinate. In order to be able to explain the experimental crystallization of **3** only, kinetic considerations may be also required.

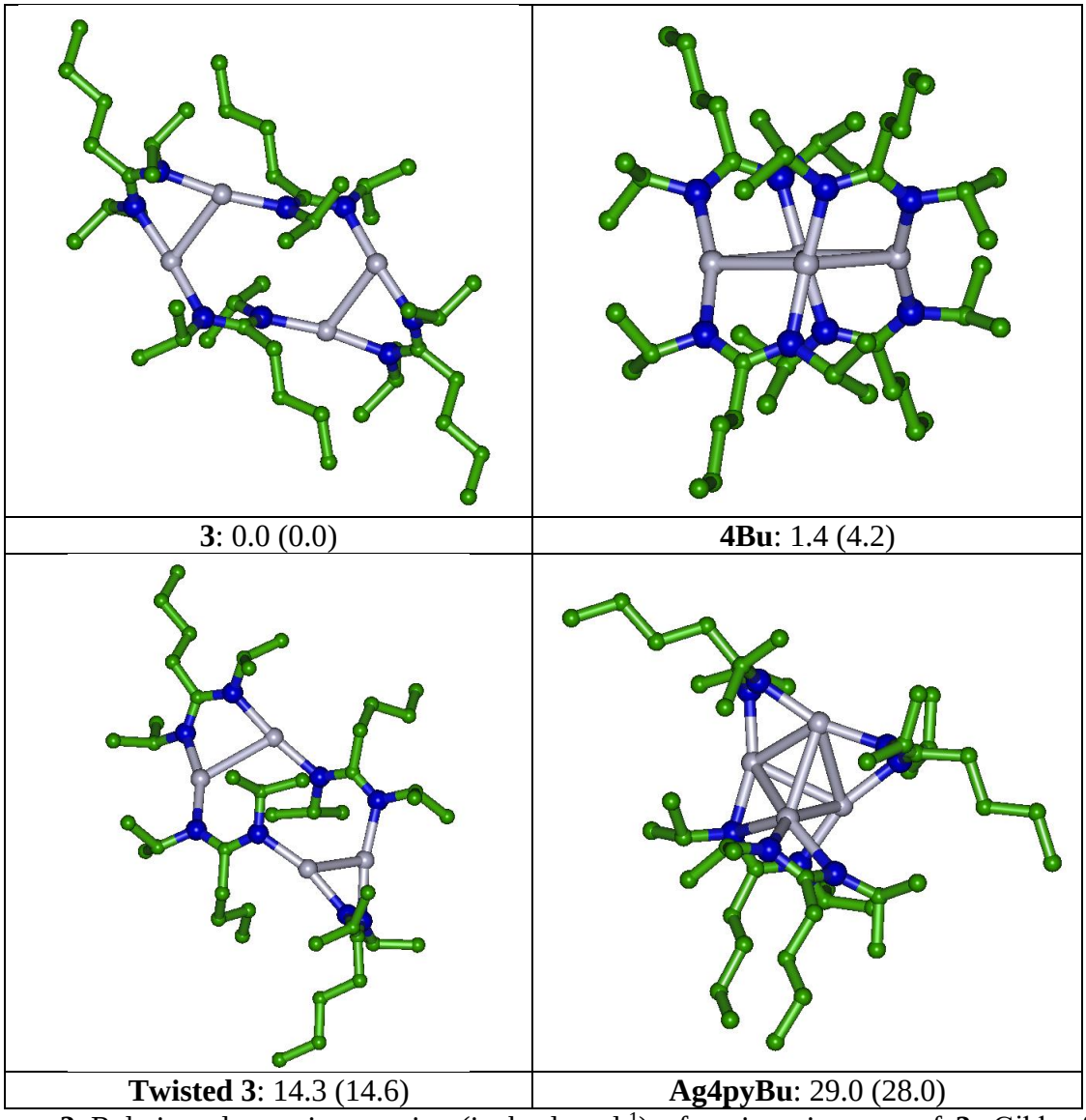

Figure 3. Relative electronic energies (in kcal mol^{-1}) of various isomers of **3**. Gibbs free energies (in kcal mol^{-1}), calculated at 298.15 K, are given in brackets. PBE-D3/def2TZVP level of calculation. Silver atoms are displayed in gray, nitrogen atoms in blue, carbon atoms in green. H atoms are omitted for clarity.

The stability of **3** and **3Me** was further studied by investigating various possible dissociation schemes (Scheme 2). The Gibbs free energies of the decomposition into a mixture of dinuclear and trinuclear complexes appears to be endergonic in the case of **3,** involving bridging diisopropyl-*n*-butylamidinate ligands (Table 1). In contrast, it appears to be almost exergonic for **3Me** involving diisopropylacetamidinate ligands (Table 1). This may explain that the Gordon's procedure is yielding a mixture of complexes **1** and **2** (and not **3Me)** for the diisopropylacetamidinate ligand, while no mixture but complex **3** only is obtained when the diisopropyl- *n*-butylamidinate ligands are involved.

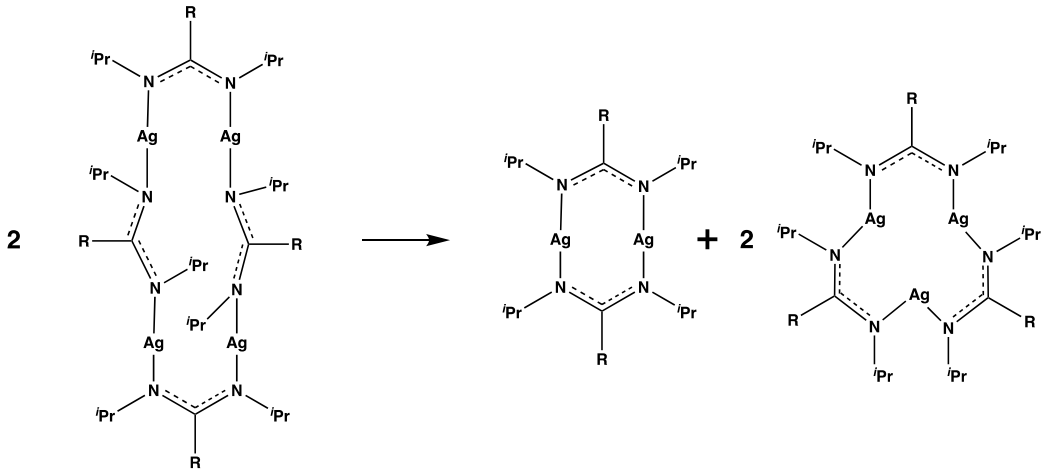

Scheme 2. Possible decomposition scheme of complex **3** and **3Me**. See Table 1 for the corresponding calculated Gibbs free energies.

Dissociation scheme	ΔE	ΔE + ZPE[a]	ΔG[b]
Scheme 2, R = Bu	32.6	31.6	10.9
Scheme 2, R = Me	18.9	17.3	1.2

Table 1. Dissociation energies of **3** and **3Me** (in kcal mol^{-1}), calculated at the PBE-D3/def2TZVP level. [a] Zero-point energy corrected value. [b] Gibbs free energies calculated at 298.15 K.

In order to further investigate the influence of the amidinate substituents on the pre-organization of the metal centers and the nuclearity of the precursor complexes, metal-ligand and metal-metal bonding (nature and strength) were finely characterized for complexes **1-4** using ELF and QTAIM topological analyses. The relevant topological descriptors will be first illustrated and described hereafter for the dinuclear silver-amidinate complex **1**, and will be subsequently discussed over the series of complexes **1-4**.

*QTAIM analysis of dinuclear silver N-N'-diisopropylacetamidinate complex **1**.*

The various QTAIM descriptors, calculated for the experimental structure of complex **1**, are shown in Table 2. While the delocalization index (DI) quantifies the degree of covalence and the multiplicity of a given bond, the bonding interactions may be characterized according to the values of local indicators of electron density and energy densities calculated at the bond critical points (BCPs) (Table 2, Figure 4).[23]

BCP [a]	ρ_{bcp}	$\Delta\rho_{bcp}$	V_{bcp} [b]	H_{bcp} [c]	$\lvert H_{bcp}\rvert/\rho_{bcp}$	$\lvert V_{bcp}\rvert/G_{bcp}$	DI [d]	E_{int} [e]
Ag1-N1	0.0918	+0.391	-0.13660	-0.0194	0.21	1.17	0.63	42.9
Ag1-N2	0.0907	+0.389	-0.13486	-0.0188	0.21	1.16	0.61	42,3
Ag1-Ag2	0.0420	+0.164	-0.05209	-0.0056	0.13	1.12	0.34	16.3

Table 2. QTAIM descriptors (in a.u.) of selected bond critical points (BCPs) involving the silver atom in complex **1**. Only the Ag-N BCPs non-equivalent through C_i symmetry are mentioned. [a]: See BCP location in Figure 4. [b]: Potential energy density V_{bcp}. [c]: Energy density H_{bcp}. [d]: Delocalization Index (DI). B3PW91/6-31G**/LANL2DZ*(Ag) level of calculation. [e]: in kcal mol^{-1}.

Negative and positive values for the Laplacian of the electron density at the BCP ($\Delta\rho_{bcp}$) are assigned to « electron-shared » and « closed-shell » interactions, respectively.[23] This classification was refined by Bianchi *et al.*[30] into three bonding regimes, depending on the value of the absolute ratio of the potential energy density to the kinetic energy density ($\lvert V_{bcp}\rvert/G_{bcp}$).

Based on the above criteria and on Macchi's recent classification,[31] the BCP descriptors related to the four Ag-N bonds are consistent with dative bonding (Table 2, Figure 4).[32] Their $\lvert V_{bcp}\rvert/G_{bcp}$ ratio refers to the intermediate region between electron-shared covalent bonds (ratio greater than 2) and closed-shell ionic bonds and van der Waals interactions (ratio lower than 1), including dative bonds and ionic bonds of weak covalent character.[25, 30] Moreover, these Ag-N bonds exhibit low electron density values ($\rho_{bcp} \approx 0.091$ a.u.) and large positive Laplacian values ($\Delta\rho_{bcp} \approx + 0.390$ a.u., Table 2). These parameters are also common to ionic bonds, but the latter display positive energy densities at the BCP (H_{bcp}), whereas these are negative in the present Ag-N interactions (Table 2).

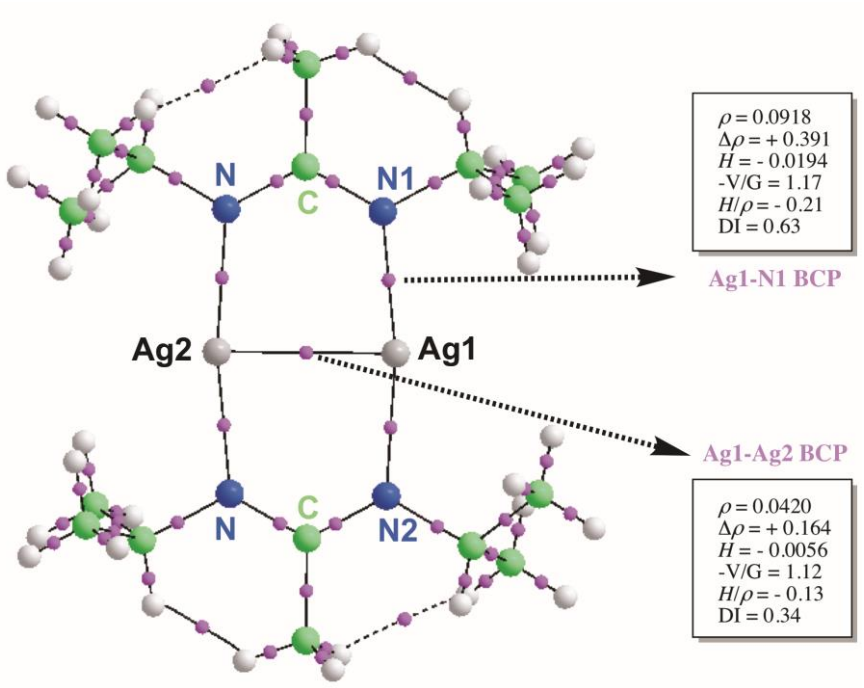

Figure 4. QTAIM molecular graph calculated at the B3PW91/6-31G**/LANL2DZ*(Ag) level for the experimental structure of complex **1**. Bond critical points are located as small magenta spheres. See main text and Table 2 for the definition of BCP descriptors.

The delocalization index (DI) values inferior to 1 are consistent with Ag-N bonds featuring a donor-acceptor character (Table 2). According to Espinosa *et al.*,[33] the "bond degree" $|\boldsymbol{H}_{bcp}|/\boldsymbol{\rho}_{bcp}$ may be useful for assigning the degree of covalence for any pairwise interaction. In complex **1**, the bond degree of Ag-N bonds ($|\boldsymbol{H}_{bcp}|/\boldsymbol{\rho}_{bcp} \approx 0.21$) is lower than the one reported at a comparable DFT calculation level (B3PW91/def2TZVP) for Cu-N bonds in both parent copper-amidinate complexes[25] and Cu-imidazole complexes[34] ($|\boldsymbol{H}_{bcp}|/\boldsymbol{\rho}_{bcp} = 0.36$), suggesting a larger ionic character of Ag-N bonds as compared to their parent Cu-N bonds. Similarly, the values of QTAIM Ag-N interaction energies ($E_{int} \approx 43$ kcal mol^{-1}) estimated through the Espinosa's correlation (Table 2),[35] are weaker than the ones of the Cu-N bonds in related copper-amidinate complexes ($E_{int} \approx 61$ kcal mol^{-1}).[25]

For the Ag-Ag interaction in **1**, the values of $|\boldsymbol{V}_{bcp}|/\boldsymbol{G}_{bcp}$ are also in the intermediate region but slightly closer to the boundary of the closed-shell region of ionic bonds. The large positive value for the Laplacian of the electron density ($\Delta\rho_{bcp} = +0.164$ a.u.) and the low electron density value (0.042 a.u.) at the Ag-Ag BCP are indicative of a ionic, closed-shell supported argentophilic Ag-Ag interaction [36] (Table 2). A weak covalent character is nevertheless, anticipated, from the sizeable value of the delocalization index (DI = 0.34, Table

2) and from the negative energy density value ($\boldsymbol{H}_{bcp}$ = -0.0056 a.u.). Both the degree of covalence, as measured by the $|\boldsymbol{H}_{bcp}|/\rho_{bcp}$ ratio (0.13), and the QTAIM Ag-Ag interaction energy (E_{int} = 16.3 kcal mol^{-1}, estimated from the Espinosa correlation, are indicative of a weakly covalent Ag-Ag argentophilic interaction. Analogous QTAIM descriptors values, were indeed recently reported by Ofori *et al.,* for the description of metallophilic Pd(II)-Pd(II) interactions [37] and of very similar argentophilic interactions to the one in **2,** in silver-imidazolecarbaldehyde oxime complexes.[26]

Although the relative strength of argentophilic and cuprophilic interactions has been the subject of debates,[38] it is noticeable that the present argentophilic interactions appear to be stronger than the cuprophilic interactions already reported for the parent dinuclear copper-(N,N'-diisopropylacetamidinate) complex.[25] Stronger argentophilic bonds as compared to cuprophilic ones, may be explained by a higher participation of Ag *s* orbitals, owing to relativistic effects. [36] The latter are also expected to increase the electron affinity of silver.[39] The latter is therefore unable to donate as much charge to a bonded anion, destabilizing geometries with anionic bridges between silver atoms and yielding silver aggregation by dispersion interactions such as argentophilic interactions.[40]

BCPs between hydrogen atoms of the methyl and isopropyl substituents of the amidinate ligands are also visible in Figure 4. Their QTAIM descriptors ($|\boldsymbol{V}_{bcp}|/\boldsymbol{G}_{bcp}$ <1, low electron density values and Laplacian, positive $\boldsymbol{H}_{bcp}$) are consistent with weak van der Waals interactions. Their large ellipticities, close to one, may indicate an approaching instability[23] and thus a very labile interaction.

*ELF analysis of dinuclear silver N-N'-diisopropylacetamidinate complex **1**.*

Ag-N and Ag-Ag interactions in the centrosymmetric experimental structure of complex **1** were further studied using ELF topological analysis. The results are shown in Figure 5 and Table 3. It is noticeable that the ELF description of both diisopropylacetamidinate ligands in **1**, is very similar to the one of the free amidinate anion (almost same populations and covariances of the ELF valence basins reported in reference 25).

	ELF descriptors		
	V(N) [a]	%Ag [b]	Cov. [c]
Ag1-N1	3.47	3.2%	-0.29
Ag1-N2	3.34	2.7%	-0.28

Ag1-Ag2	-	-	-0.16

Table 3. ELF descriptors of the inequivalent Ag-N bonds and of the Ag-Ag interaction in complex **1** (experimental geometry). [a]: Average population $\bar{N}$ of the ELF valence basin V(N) (in e^-) [b]: QTAIM atomic contribution of Ag to V(N). [c]: covariance $< \bar{\sigma}^2(V(N), C(Ag))>$. B3PW91/6-31G**/LANL2DZ*(Ag) level of calculation.

Each silver core basin, C(Ag) is surrounded by two monosynaptic valence basins V(N), that may be related to the Ag-N bonds with both amidinate ligands. The QTAIM atomic contributions of Ag to the population of these basins are weak but sizeable, about 3% (Table 3). The V(N) attractor is located at 0.615 Å from the C(N) attractor, i.e. about one third of the Ag-N distance, closer to N than in the free amidinate anion (0.715 Å). According to the literature, these features, along with the large negative covariance $< \sigma^2(V(N), C(Ag)) > = -0.28$, are consistent with Ag-N dative bonds. **25**,41 The weak QTAIM atomic contribution of Ag to V(N), i.e. lower than 10% of the V(N) basin population, is indicative of dative Ag-N bonds, exhibiting a strong ionic character, as illustrated in the most representative mesomeric form shown in Figure 5.

Although the QTAIM atomic charge of Ag centers is only + 0.6 (Figure 5), the formal oxidation state of the silver atom estimated from ELF analysis is found to be 0.8, thus close to +I. This is calculated by subtracting the effective population of the C(Ag) basin from the expected number of explicit electrons from Ag involved in the electronic structure calculation, namely 19 electrons, as a small-core pseudo-potential was used to describe the Ag atoms.

The metallophilic interaction in the parent dinuclear copper-amidinate complex was characterized by a disynaptic V(Cu,Cu) basin and two monosynaptic V(Cu) basins,**25** In contrast, in **1**, there is no disynaptic V(Ag,Ag) basin. The argentophilic interaction is supported by the large negative covariance (-0.16) between both Ag core basins C(Ag) only. This is a charge-shift type bonding already highlighted in various metal-metal bonds. **25**

These results are in agreement with the above QTAIM description of Ag-N and Ag-Ag-Ag interactions in **1**.

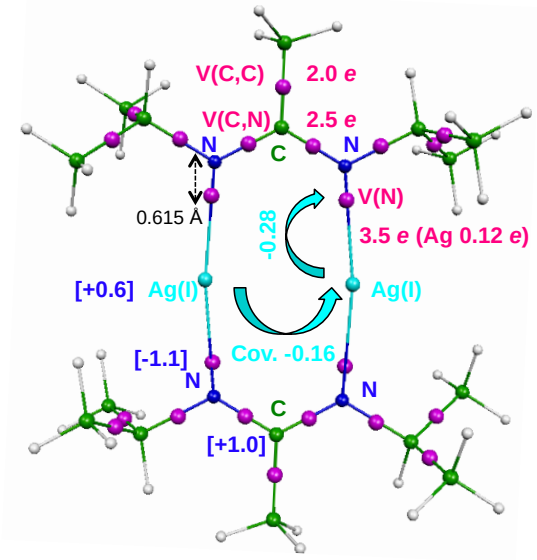

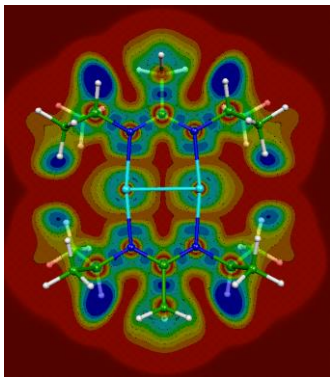

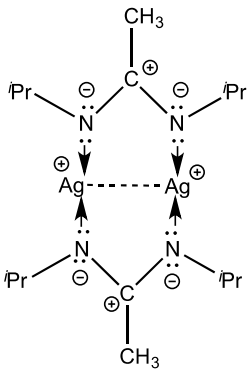

Map of ELF attractors of **1**	ELF map in the N-Ag-N plane	Mesomeric form

Figure 5. ELF analysis of silver complex **1**. ELF attractors are located as small magenta spheres and the average populations of the corresponding ELF basins are displayed in magenta. QTAIM atomic charges are shown in blue brackets and covariances between ELF basins are displayed in cyan color. B3PW91/6-31G**/LANL2DZ*(Ag) level of calculation.

*Comparison of relevant QTAIM and ELF descriptors of silver complexes **1-4***

ELF and QTAIM analyses were also performed for complexes **2-4**. The relevant ELF and QTAIM descriptors are listed in Tables S2-S7 in the supporting information.

The QTAIM descriptors of the Ag-N BCPs are very similar over the **1-4** series. They are referring to the intermediate bonding regime ($|\boldsymbol{V}_{\mathbf{bcp}}|/\boldsymbol{G}_{\mathbf{bcp}} \approx 1.16$), to a similar covalence degree as measured by both DI ≈ 0.60 and $|H_{bcp}|/\rho_{bcp} \approx 0.20$, and thus to dative Ag-N bonds of similar strength over the series as indicated by E_{int} (40 - 44 kcal mol^{-1} range).

Similarly, the ELF relevant descriptors of the Ag-N bonds are lying in the same range over the series (Tables S2-S7). However, while the QTAIM descriptors of "*cis*"-bridging and "*trans*"-bridging amidinate ligands in **3** are the same, both the slightly larger QTAIM contribution to the population of the ELF V(N) basin (4.7% versus 3.3%) and the larger covariance in absolute value ($<\sigma^2(V(N), C(Ag))> = -0.29$ versus -0.26) are in favor of a slightly larger covalence degree and strength of Ag-N bonds in the "cis" bridging mode (Table S5).

In contrast to Ag-N bonds, argentophilic interactions of various strengths may be characterized over the **1-4** series.

In the trinuclear complex **2**, only two argentophilic interactions may be found, corresponding to the Ag1-Ag2 and Ag2-Ag3 distances of 2.86 and 2.90 Å respectively (Table 4 and Table S2). They are about half-weaker than the argentophilic interaction in **1** (E_{int} ≈ 7-8 kcal mol^{-1} versus 16.3 kcal mol-1). A much weaker Ag1-Ag3 ionic interaction ($|\boldsymbol{V}_{bcp}|/\boldsymbol{G}_{bcp}$ = 0.98 <1, positive $\boldsymbol{H}$ value, ELF covariance < $\bar{\sigma}^2$(C(Ag), C(Ag))> ≈ 0) is also characterized. Both argentophilic interactions exhibit similar DI and $|\boldsymbol{H}_{bcp}|/\boldsymbol{\rho}_{bcp}$ ratio values, smaller than the one of the argentophilic interaction in **1** (Table 1), suggesting a lower covalence degree (Table 4).

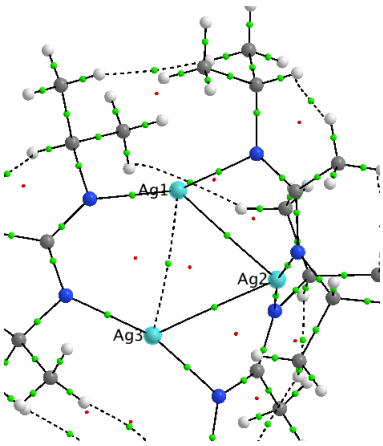

QTAIM molecular graph

	Ag1-Ag2	Ag2-Ag3	Ag1-Ag3
Distance	2.86	2.90	3.20
$\boldsymbol{H}_{bcp}$	-0.00094	-0.00058	+ 0.00017
$\lvert\boldsymbol{H}_{bcp}\rvert/\boldsymbol{\rho}_{bcp}$	0.03	0.02	0.01
DI	0.24	0.21	0.11
E_{int} [b]	8.0	7.1	3.0
Covariance [a]	-0.11	-0.09	-0.04
E^{IQA}_{int} [b]	-0.06	3.47	13.14
V^{IQA}_{cl} [b]	25.46	25.91	24.04
V^{IQA}_{xc} [b]	-25.53	-22.44	-10.89

Table 4. Comparison of Ag-Ag distances (in Å) and of the relevant ELF and QTAIM descriptors (in a.u.) of Ag-Ag interactions in **2**. See atom labeling on the QTAIM molecular graph. [a]: ELF covariance < $\bar{\sigma}^2$(C(Ag), C(Ag))>. B3PW91/6-31G**/LANL2DZ*(Ag) level of calculation. [b]: Interaction energy in kcal mol^{-1}

The IQA analysis is expected to refine the above ELF and QTAIM description of the Ag-Ag interactions in **2** especially their covalence degree and their stabilizing or repulsive nature. For the shorter Ag1-Ag2 distance, the exchange-correlation IQA energy contribution (V^{IQA}_{xc}) is slightly larger than the classical coulombic contribution (V^{IQA}_{cl}), in agreement with the stabilizing argentophilic interaction of weak covalence degree suggested by other ELF and

QTAIM descriptors (Table 4). In contrast, for both Ag2-Ag3 and Ag1-Ag3, the IQA electrostatic contribution is larger than the exchange-correlation component resulting in positive E^{IQA}_{int} values, thus non-stabilizing interactions (Table 4).

Two identical argentophilic interactions of the same covalence degree (DI = 0.25 and $|\boldsymbol{H}_{bcp}|/\rho_{bcp}$ = 0.04) and strength (E_{int} = 8.4 kcal mol^{-1}) are found in the centrosymmetric silver complex **3** (Table 5). From both the QTAIM and ELF descriptors, these Ag-Ag interactions are very similar to the Ag1-Ag2 interaction described above in **2** (Table 4).

	Ag-Ag
Distance	2.85
$\boldsymbol{H}_{bcp}$	-0.00108
$\lvert\boldsymbol{H}_{bcp}\rvert/\rho_{bcp}$	0.04
DI	0.25
E_{int} (kcal mol^{-1})	8.4
Covariance [a]	-0.11

Table 5. Comparison of ELF and QTAIM descriptors (in a.u.) of the argentophilic interaction in **3**. [a]: ELF covariance $< \bar{\sigma}^2(C(Ag), C(Ag))>$. B3PW91/6-31G**/LANL2DZ*(Ag) level of calculation.

Four argentophilic interactions are characterized in complex **4** (Table 6). They are similar in covalence degree and strength (E_{int} ranging from 6.9 to 7.5 kcal mol^{-1}) (Table 6). Their covalence degree and strength are however little smaller than in **2** and **3**.

	Ag1-Ag2	Ag2-Ag3	Ag1-Ag3	Ag3-Ag4	Ag4-Ag1
Distance	2.91	2.88	3.12	2.87	2.91
$\boldsymbol{H}_{bcp}$	-0.00064	-0.00087	+ 0.00005	-0.00084	-0.00057
$\lvert\boldsymbol{H}_{bcp}\rvert/\rho_{bcp}$	0.02	0.03	0.00	0.03	0.02
DI	0.23	0.22	0.14	0.24	0.21
E_{int} (kcal mol^{-1})	7.0	7.7	3.9	7.5	6.9
Covariance [a]	-0.10	-0.12	-0.06	-0.10	-0.10

Table 6. Comparison of Ag-Ag distances (in Å) and of relevant ELF and QTAIM descriptors (in a.u.) of Ag-Ag interactions in **4**. [a]: ELF covariance $< \bar{\sigma}^2(C(Ag), C(Ag))>$. B3PW91/6-31G**/LANL2DZ*(Ag) level of calculation.

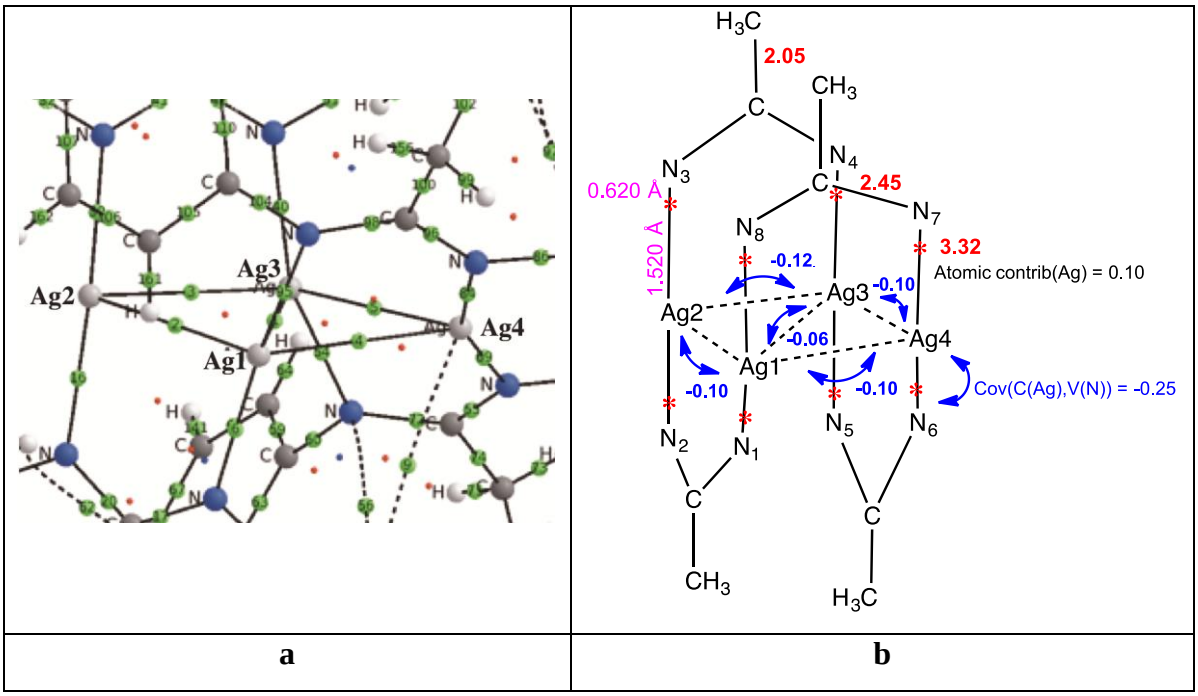

a **b**

Figure 6a. Part of the QTAIM molecular graph of **4**. **Figure 6b.** ELF analysis of tetranuclear silver complex **4**. ELF attractors (small stars) and their populations are highlighted in red. Values of covariances between C(Ag) core basins are displayed over blue arrows. B3PW91/6-31G**/LANL2DZ*(Ag) level of calculation.

The relevant ELF and QTAIM descriptors of the stronger argentophilic interactions in the **1**-**4** series, are summarized in Table 7. Those of complexes **2-4** are very similar suggesting the same covalence degree and strength of the corresponding Ag-Ag interactions, about half-weaker than in **1**, in which the Ag-Ag distance is also much lower.

The IQA analysis allows for refining the description of the stronger argentophilic interactions in the **1-3** series. The negative E^{IQA}_{int} values are consistent with stabilizing interactions. The exchange-correlation IQA energy components are always slightly larger than the classical energy ones along the **1-3** series (Table 7). This is consistent with the corresponding sizeable covalence degrees, suggested by the $|\boldsymbol{H}_{bcp}|/\boldsymbol{\rho}_{bcp}$ values. However, E^{IQA}_{int} values appear to be much lower than Espinosa's E_{int} interaction energies, suggesting different meanings.

	1	2	3	4
Distance	2.65	2.86	2.85	2.87
H_{bcp}	-0.00056	-0.00094	-0.00108	-0.00084
$\lvert H_{bcp} \rvert / \rho_{bcp}$	0.13	0.03	0.04	0.03
DI	0.34	0.24	0.25	0.24
Covariance[a]	-0.16	-0.11	-0.11	-0.10
E_{int} [b]	16.3	8.0	8.4	7.5
E^{IQA}_{int} [b]	-7.35	-0.06	-0.78	na
V^{IQA}_{cl} [b]	30.77	25.46	26.01	na
V^{IQA}_{xc} [b]	-38.12	-25.53	-26.79	na

Table 7. Comparison of Ag-Ag distances (in Å) and of relevant ELF and QTAIM descriptors (in a.u.) of the stronger argentophilic interactions in the **1-4** series. [a]: ELF covariance $< \bar{\sigma}^2(C(Ag), C(Ag))>$. [b]:Interaction energy in kcal mol^{-1}. B3PW91/6-31G**/LANL2DZ*(Ag) level of calculation.

Conclusion

The crystal structure of tetranuclear silver-(N-N'-diisopropyl-n-butylamidinate) (**3**) has been disclosed here. This new silver amidinate precursor has been already used for the preparation of AgNPs in devices for the electrochemical detection of aqueous pollutant. [20] The properties of this new silver-amidinate precursor will be further studied for the synthesis of colloidal AgNPs and their assemblies.

Preliminary DFT studies of the relative stabilities and possible dissociation schemes of various isomeric arrangements of silver atoms in **3**, have given insight into the role of the methyl or *n*-butyl substituents on the nuclearity and stability of the related silver-amidinate complexes.

The metal-ligand and metal-metal interactions in **3** and in a series of related silver amidinate complexes **1-4**, have been finely characterized using ELF and QTAIM topological analyses. The Ag-N dative bonds, exhibiting a strong ionic character, are very similar over the series but weaker than related Cu-N dative bonds. [25]

In contrast, argentophilic interactions of various strength and covalence degree are characterized in the **1-4** series. As already highlighted in a previous report, [41] the Ag-Ag distances and the relevant ELF and QTAIM descriptors of the strength (E_{int}) and covalence degree (DI, $\lvert H \rvert / \rho$, absolute value of ELF covariance) of all argentophilic interactions in the **1-4** series are correlated either linearly or using a logarithmic fit (Figure 7). All of them appear

therefore as relevant descriptors for the characterization of the covalence degree of argentophilic interactions.

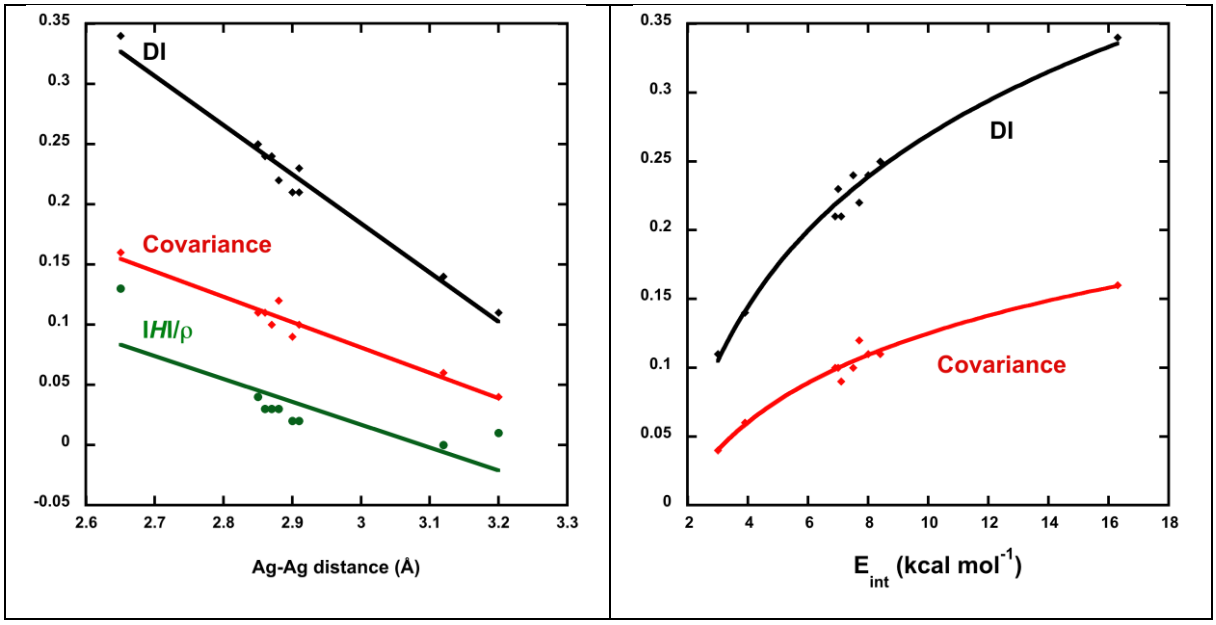

Figure 7. Correlations between ELF and QTAIM descriptors of the strength (E_{int}) and covalence degree (DI, $|H|/\rho$, absolute value of ELF covariance) of all argentophilic interactions in the **1**-**4** series.

It is noticeable that the argentophilic interaction in **1** is about twice stronger than the ones in the **2**-**4** series. Various reduction mechanisms and nucleation schemes may therefore envisionned for the **1**-**4** series, depending on the pre-organization of the silver centers *via* their argentophilic interactions in the precursor complex. Preliminary studies of the monoelectronic reduction of precursors **1**-**3** have indeed shown that their reduction proceed in very different pathways.

Experimental section

Materials and reagents.

All experiments were performed under argon atmosphere using either glovebox or standard Schlenk techniques. Glassware was oven-dried at 383 K prior to use. Solvents were obtained from a solvent purification system (Braun). *n*-butyllithium (Aldrich) was used as received.

Preparation of Silver N-N'-diisopropyl-n-butylamidinate (3)[20]

1.2 molar equivalent of a 2.5 mol L^{-1} *n*-butyllithium solution in hexane was added dropwise to an N, N'-diisopropylcarbodiimide solution (0.34 mmol L^{-1} in dry diethyl ether) cooled below -80°C. The latter was stirred for 10 mn, then allowed to warm back to room temperature (RT) and stirred again during 4 hours at RT. The colourless solution turned to pale yellow. Away from light, the latter solution was poured into a suspension of 1.2 equivalent of AgCl (0.50 mmol L^{-1} in diethylether). The mixture turned rapidly black and was stirred away from light overnight.

The latter black solution was then dried under vacuum away from light, until a black solid was obtained. This solid was washed four times with 10 mL of dry *n*-pentane on a glass filter to yield a clear strong orange solution. This solution was left at -40°C for a week to allow recrystallization. White crystals were obtained with a typical yield of 40 %.

X-ray Structural Determination

Crystals were kept away from air and light until they were dipped into Fomblin oil for their selection.

Data were collected at low temperature (100 K) on a KappaCCD Nonius diffractometer using a graphite-monochromated Mo-Kα radiation (λ = 0.71073Å) and equipped with an Oxford Cryosystems Cryostream Cooler Device. The structures have been solved by Direct Methods using SHELXS-97[42] and refined by means of least-squares procedures on a F^2 with the aid of the program CRYSTALS.[43] The Atomic Scattering Factors were taken from International tables for X-Ray Crystallography.[44] All hydrogens atoms were placed geometrically, and refined by using a riding model.

All non-hydrogens atoms were anisotropically refined, and in the last cycles of refinement a weighting scheme was used, where weights are calculated from the following formula: $w=1/[\sigma^2(Fo^2) + (aP)^2 + bP]$ where $P = (Fo^2 + 2Fc^2)/3$.

Drawings of molecules were performed with the program ORTEP32[45] with 30% probability displacement ellipsoids for non-hydrogen atoms.

Complete details of the X-ray analysis reported herein have been deposited at the Cambridge Crystallographic Data Centre (CCDC 1957857 (**3**)). This data can be obtained free of charge via www.ccdc.cam.ac.uk/ data_request/cif, or by e-mailing data_request@ccdc.cam.ac.uk, or by contacting the Cambridge Crystallographic Data Centre, 12, Union Road, Cambridge CB2 1EZ, U.K.; fax: +44 1223 336033.

Computational details

Geometries were fully optimized at the PBE-D3/def2TZVP level of calculation using Gaussian09. [46] Vibrational analysis was performed at the same level as the geometry optimization. Solvent effects of THF (ε = 7.4257) were included using the polarizable continuum model (PCM) implemented in Gaussian09. Dispersion-corrected DFT (DFT-D) methods have been shown to be more suitable than second-order Moller-Plesset (MP2) perturbation theory calculations for the description of argentophilic interactions. The strength of the latter is comparable to the one of hydrogen bonds. MP2 calculations tend to overestimate them.[39,40]

Electron Localization Function (ELF) [24,] [47] topological analysis and Quantum Theory of Atoms in Molecules (QTAIM) analysis were performed on the experimental geometries with the TopMoD package [48] at the B3PW91/6-31G**/LANL2DZ*(Ag). The star in LANL2DZ*(Ag) refers to *f*-polarization functions derived by Ehlers *et al.*[49] for Ag, that have been added to the LANL2DZ(Ag) basis set. ELF maps were plotted using the Molekel program.[50] QTAIM[23] and IQA[51] analyses were performed with the AIMAll software.[52]

Topological analyses. Topological methods are based on the analysis of the gradient field of a local function within the dynamic field theory and provide a partition of the molecular space into non-overlapping basins.

The topological analysis of the electron density $\rho(r)$, designed as the Quantum Theory of Atoms in Molecules (QTAIM) by R. Bader, yields atomic basins and QTAIM atomic charges. [23] It allows defining bond paths and bond critical points (BCPs). The nature of the chemical bond is characterized from various properties of the electron density at the BCPs, especially the sign of the Laplacian of the electron density and the values of the kinetic energy density (G_{bcp}), of the potential energy density (V_{bcp}) and of the energy density $H_{bcp} = G_{bcp} + V_{bcp}$ following the Macchi's classification.[31] The covalence degree may be estimated from H_{bcp}/ρ_{bcp}. [33] The strength of the interaction may be estimated from the correlation scheme of Espinosa *et al.* and the corresponding positive interaction energy ($E_{int} = - ½ V_{bcp}$). [35] IQA analysis was performed to get insight into the relative contributions of electron sharing and electrostatic interactions of the argentophilic interactions of complexes **1**-**3**. Within the IQA energy decomposition scheme, using QTAIM atoms, the total energy of the system is decomposed into intra-atomic and interatomic contributions. The interatomic interactions energy, E^{IQA}_{int} (A,B) (A ≠ B), is further partitioned as E^{IQA}_{int} (A, B) = V^{IQA}_{cl} (A, B) + V^{IQA}_{xc} (A, B). V^{IQA}_{cl} (A, B), called the classical

term, is related to the electrostatic component of the A-B interaction, while V^{IQA}_{xc} (A, B), known as the exchange-correlation term, refers to electron sharing due to quantum mechanic effects that also incorporate Pauli Exclusion Principle and may be related to the covalence degree of the bond. IQA analyses have been shown to be useful for characterizing non-covalent intereactions.[53]

The electron localization function (ELF) measures the excess of kinetic energy due to the Pauli repulsion. [24, 47] ELF values are confined between 0 and 1. ELF tends to a value of 1 in those regions where the electron localization is high (atomic shells, chemical bonds, and single electron or lone pairs) whereas it tends towards small values at the boundaries between these regions. [54,55] The topological analysis of the ELF gradient field yields a partition of the molecular space into non-overlapping electronic domains, classified into core, valence bonding and nonbonding basins. These basins are in one-to-one correspondence to the core, lone or shared pairs of the Lewis model. A core basin contains a nucleus X (except a proton) and is designated as C(X). A valence basin lies between two or more core basins. Valence basins are further distinguished by their synaptic order, which is the number of core basins with which they share a common boundary. The monosynaptic basins denoted as V(X), correspond to lone pairs, whereas the di- and polysynaptic ones are related to bi- or multi-centric bonds, denoted as V(X1, X2, X3, ...). The average population of the basin is obtained by integration of the one-electron density over the basin volume. These populations do not take integral values and are about twice the topologically defined Lewis bond orders for bonding valence basins. The populations and (co)variances of these valence basins can be further interpreted in terms of weighted combinations of mesomeric structures.[56]

Supporting Information.

Crystallographic information for complex **3**. Complementary computational data. ELF and QTAIM descriptors for complexes **2-4**.

Author Information

ORCID

Maxime Puyo: 0000-0001-9662-3293

Laure Vendier: 0000-0002-7111-9258

Myrtil L Kahn: 0000-0003-3079-5759

Pierre Fau: 0000-0003-0014-2511

Katia Fajerwerg: 0000-0002-3897-3380

Christine Lepetit: 0000-0002-0008-9506

Acknowledgements. The theoretical studies were performed using HPC resources from CALMIP (Grant 2016-2019 [0851]]) and from GENCI-[CINES/IDRIS] (Grant 2016-2019 [085008]). The authors wish to acknowledge the financial support of the Centre National de la Recherche Scientifique (CNRS) and the Ministère de l'Enseignement Supérieur, de la Recherche et de l'Innovation (MESRI).

References

[1] Burdusel, A. -C.; Gherasim, O.; Grumezescu, A. M.; Mogoanta, L.; Ficai, A.; Andronescu, E. Biomedical applications of silver nanoparticles: an up-to-date overview. *Nanomaterials* **2018**, *8*, 681/1-25.

[2] Lee, J.-S. Silver nanomaterials for the detection of chemical and biological targets. *Nanotechnol. Rev.* **2014**, *3*, 499-513.

[3] Ueno, K.; Oshikiri, T.; Sun, Q.; Shi, X.; Misawa, H. Solid-State Plasmonic Solar Cells. *Chem. Rev.* **2018,** *118*, 2955-2993.

[4] Kaur, R.; Bariwal, J.; Voskressensky, L. G.; Van der Eycken, E. V. Gold and silver nanoparticle-catalyzed synthesis of heterocyclic compounds. *Chemistry of Heterocyclic Compounds* **2018**, *54*, 241-248.

[5] Kolobova, E. N.; Pestryakov, A. N.; Bogdanchikova, N.; Cortes Corberan, V. Silver catalysts for liquid-phase oxidation of alcohols in green chemistry: challenges and outlook. *Catal. Today* **2019**, *333*, 81-88.

[6] Khatoon, U. T.; Rao, G. V. S. N.; Mantravadi, K. M.; Oztekin, Y. Strategies to synthesize various nanostructures of silver and their applications - a review. *RSC Advances* **2018**, *8*, 19739-19753.

[7] Crawford, S. E.; Hartmann, M. J. ; Millstone, J. E. Surface Chemistry-Mediated Near-Infrared Emission of Small Coinage Metal Nanoparticles. *Acc. Chem. Res.* **2019**, *52*, 695-703.

[8] Lea, M. C. On allotropic forms of Silver. *Am. J. Sci.* **1889**, *37*, 476-491.

[9] Iravani, S.; Zolfaghari, B.; Korbekandi, H.; Mirmohammadi, S. V. Synthesis of silver nanoparticles: chemical, physical and biological methods. *Res. Pharmaceutical Sci.* **2014**, *9*, 385-406.

[10] Tan, K. S.; Cheong, K. Y. Advances of Ag, Cu, and Ag-Cu alloy nanoparticles synthesized via chemical reduction route. *J. Nanoparticle Res.* **2013**, *15*, 1537/1-1537/29.

[11] Zhou, S.; Zhao, M.; Yang, T.-H.; Xia, Y. Decahedral nanocrystals of noble metals: synthesis, characterization, and applications. *Materials Today* **2019**, *22*, 108-131.

[12] Sun, Y. Controlled Synthesis of Colloidal Silver Nanoparticles in Organic Solutions: Empirical Rules for Nucleation Engineering. *Chem. Soc. Rev.* **2013**, *42*, 2497−2511.

[13] Andrieux-Ledier, A.; Tremblay, B.; Courty, A., Synthesis of Silver Nanoparticles Using Different Silver Phosphine Precursors: Formation Mechanism and Size Control. *J. Phys. Chem. C* **2013,** *117*, 14850-14857.

[14] Tang, Y.; Ouyang, M. Tailoring properties and functionalities of metal nanoparticles through crystallinity engineering. *Nature Mater.* **2007**, *6* , 754-759.

[15] Ouhenia-Ouadahi, K.; Andrieux-Ledier, A.; Richardi, J.; Albouy, P. A.; Beaunier, P.; Sutter, P.; Sutter, E.; Courty, A. Tuning the Growth Mode of 3D Silver Nanocrystal Superlattices by Triphenylphosphine. *Chem. Mater.* **2016**, *28*, 4380-4389.

[16] Archibald, S. J.; Alcock, N. W.; Busch, D. H.; Whitcomb, D. R. Synthesis and characterization of silver(I) complexes with C-alkyl functionalized N,N'-diphenylamidinates: tetrameric and trimeric structural motifs. *J. Cluster Sci.* **2000**, *11*, 261-282.

[17] (a) Li, Z.; Rahtu, A.; Gordon, R. G. Atomic Layer Deposition of Ultrathin Copper Metal Films from a Liquid Copper(I) Amidinate Precursor. *J. Electrochem. Soc.* **2006**, *153*, C787-C794. (b) Barrière, C.; Piettre, K.; Latour, V.; Margeat, O.; Turrin, C.-O.; Chaudret, B.; Fau, P. Ligand effects on the air stability of copper nanoparticles obtained from organometallic synthesis. *J. Mater. Chem.* **2012**, *22*, 2279-2285.

[18] Lim, B. S.; Rahtu, A.; Park, J.-S.; Gordon, R. G. Synthesis and characterization of volatile, thermally stable, reactive transition metal amidinates. *Inorg. Chem.* **2003**, *42*, 7951-7958.

[19] Cure, J.; Coppel, Y.; Dammak, T.; Fazzini, P. F.; Mlayah, A.; Chaudret, B.; Fau, P. Monitoring the Coordination of Amine Ligands on Silver Nanoparticles Using NMR and SERS. *Langmuir* **2015,** *31*, 1362-1367.

[20] Puyo, M.; Fau, P.; Kahn, M. L.; Mesguich, D.; Launay, J.; Fajerwerg, K. Removable composite electrode made of silver nanoparticles on pyrolyzed photoresist film for the electroreduction of 4 nitrophenol. *Langmuir* **2019**, DOI: 10.1021/acs.langmuir.9b02405.

[21] Hsu, W.; Yang, X.-K.; Chhetri, P. M.; Lin, S.-J.; Li, Y.-S.; Chen, T.-R.; Chen, J.-D.; Au(I) and Ag(I) formamidinate tetranuclear complexes and coordination polymers: Synthesis, structures and luminescent properties. *Inorg. Chim. Acta* **2018**, *482*, 785-790.

[22] Tong, L.; Davis, L. M.; Gong, X.; Feng, J.; Beh, E.S.; Gordon, R.G. Synthesis of volatile, reactive coinage metal 5,5-bicyclic amidinates with enhanced thermal stability for chemical

vapor deposition. *Dalton Trans.* **2019**, 48, 6709-6713.

[23] (a) Bader, R. F. W. in *Atoms In Molecules*, **1990**, Clarendon Press: Oxford, UK. (b) Bader, R. F. W.; Essen, H. The characterization of atomic interactions. *J. Chem. Phys.* **1984**, *80*, 1943-1960.

[24] Silvi, B.; Savin, A. Classification of chemical bonds based on topological analysis of electron localization function, *Nature* **1994**, *371*, 683–686.

[25] Lepetit, C.; Fau, P.; Fajerwerg, K.; Kahn, M. L.; Silvi, B. Topological analysis of the metal-metal bond: a tutorial review. *Coord. Chem. Rev.* **2017**, *345*, 150-181.

[26] Ofori, A.; Suvanto, S.; Jääskeläinen, S.; Koskinen, L.; Koshevoy, I. O.; Hirva, P. Versatile coordination modes in silver-imidazolecarbaldehyde oxime complexes: structural and computational analysis. *Cryst. Growth Des.* **2016**, *16*, 255−264.

[27] https://www.ccdc.cam.ac.uk/.../ccdcresources/Elemental_Radii.xlsx (Cambridge Structural Database**)**. Van der Waals radii are taken from A. Bondi, *J. Phys. Chem.* **1964**, *68*, 441-452 except the value for H, which is taken from R. S. Rowland & R. Taylor, *J. Phys. Chem.* **1996**, *100*, 7384-7391. Radii that are not available in either of these publications have RvdW = 2.00 Å.

[28] Irwin, M. D.; Abdou, H. E.; Mohamed, A. A.; Fackler, J. P. Jr. Synthesis and X-ray structures of silver and gold guanidinate-like complexes. A Au(II) complex with a 2.47 Å Au–Au distance. *Chem. Commun.* **2003**, 2882-2883.

[29] Schuerman, J. A.; Fronczek, F. R.; Selbin, J. New Silver Cluster Compounds Containing Dithiobenzoate Ligand. *Inorg. Chim. Acta*, **1989**, *160*, 43-52.

[30] Bianchi, R.; Gervasio, G.; Marabello, D. Experimental Electron Density Analysis of $Mn_2(CO)_{10}$: Metal-Metal and Metal-Ligand Bond Characterization. *Inorg. Chem.* **2000**, *39*, 2360-2366.

[31] Macchi, P.; Proserpio, D.M.; Sironi, A. Experimental Electron Density in a Transition Metal Dimer: Metal-Metal and Metal-Ligand Bonds. *J. Am. Chem. Soc.* **1998**, *120*, 13429-13435.

[32] For a classification of various ligands see: Green, M. L. H. A new approach to the formal classification of the covalent compounds of the elements. *J. Organomet. Chem.* **1995**, *500*, 127-148.

[33] Espinosa, E.; Alkorta, I.; Elguero, J.; Molins, E. From weak to strong interactions: A comprehensive analysis of the topological and energetic properties of the electron density distribution involving X–H …F–Y systems. *J. Chem. Phys.* **2002**, *117*, 5529-5542.

[34] Boukallaba, M.; Kerkeni, B.; Lepetit, C.; Berthomieu, D. Coordination complexes of 4-Methylimidazole with Zn^{II} and Cu^{II} in gas phase and in water: A DFT Study. *J. Mol. Model.* **2016**, *22*, 301/1-10.

[35] (a) Espinosa, E.; Molins, E.; Lecomte, C. Hydrogen bond strengths revealed by topological analyses of experimentally observed electron densities. *Chem. Phys. Lett.* **1998**, *285*, 170-173. (b) Espinosa, E.; Alkorta, I.; Rozas, I.; Elguero, J.; Molins, E. About the evaluation of the local kinetic, potential and total energy densities in closed-shell interactions. *Chem. Phys. Lett.* **2001**, *336*, 457-461. $E_{int} = - ½ V_{bcp}$ and E_{int} (kcal mol-1) = -313.754 x V_{bcp} (au)

[36] Schmidbaur, H.; Schier, A. Argentophilic interactions. *Angew. Chem. Int. Ed.* **2015**, *54*, 746-784.

[37] (a) Estevan, F.; Ibáñez, S.; Ofori, A.; Hirva, P.; Sanaú, M.; Úbeda, M. A. Benzoato and Thiobenzoato Ligands in the Synthesis of Dinuclear Palladium(III) and -(II) Compounds: Stability and Catalytic Applications. *Eur. J. Inorg. Chem.* **2015**, 2822-2832. (b) Estevan, F.; Hirva, P.; Ofori, A.; Sanaú, M.; Spec, T.; Úbeda, M. A. Pyrazole and Pyrazolate as Ligands in the Synthesis and Stabilization of New Palladium(II) and (III) Compounds. *Inorg. Chem.* **2016**, *55*, 2101-2113.

[38] (a) Wong, K.M.-C.; Au, V.K.-M.; Yam, V.W.-W. *Comprehensive Inorganic Chemistry II From Elements to Applications*, Coordination and Organometallic Chemistry, 2nd edn, vol. 8, Elsevier, Amsterdam, **2013**, pp. 59-130. (b) Ray, L.; Shaikh, M. M.; Ghosh, P. Shorter argentophilic interaction than aurophilic interaction in a pair of dimeric $\{(NHC)MCl\}_2$ (M = Ag, Au) complexes supported over a N/O-functionalized N-heterocyclic carbene (NHC) ligand. *Inorg. Chem.*, **2008**, *47*, 230-240. (c) O'Grady, E.; Kaltsoyannis, N. Does metallophilicity increase or decrease down group 11? Computational investigations of $[Cl–M–PH_3]_2$ (M = Cu, Ag, Au, [111]). *Phys. Chem. Chem. Phys.* **2004**, *6*, 680-687; (d) Poblet, J.-M.; Bénard, M. Cuprophilicity, a still elusive concept: a theoretical analysis of the ligand-unsupported Cu^I-Cu^I interaction in two recently reported complexes. *Chem. Commun.* **1998**, 1179-1180.

[39] Riedel, S.; Pyykko, P.; Mata, A. C.; Werner, H.-J. Comparative calculations for the A-frame molecules $[S(MPH_3)_2]$ (M = Cu, Ag, Au) at levels up to CCSD(T). *Chem. Phys. Lett.* **2005**, *405*, 148–152.

[40] Otero-de-la-Roza, A.; Mallory, J. D.; Johnson, E. R. Metallophilic interactions from dispersion-corrected density-functional theory. *J. Chem. Phys.* **2014**, *140*, 18A504/1-10.

[41] Lepetit, C.; Vabre, B.; Canac, Y.; Alikhani,M. E.; Zargarian, D. Pentacoordinated, Square-Pyramidal Cationic PCP Ni(II) Pincer Complexes: ELF and QTAIM Topological Analyses of Nickel-Triflate Interactions *Theor. Chem. Acc.* **2018**, *137*: 141/1-22.

[42] Sheldrick, G. M. A short history of SHELX. *Acta Cryst. A: Foundations of Crystallography* **2008,** *64*, 112-122.

[43] CRYSTALS version 12: software for guided crystal structure analysis. Betteridge, P.W.; Carruthers, J. R.; Prout, K.; Watkin, D. J. *J. Appl. Cryst.* **2003**, *36*, 1487.

[44] Ibers, J. A.; Hamilton, W. C.; Editors, *International Tables for X-Ray Crystallography, Vol. 4: Revised and Supplementary Tables to Volumes 2 and 3*. **1974**; p 366.

[45] Farrugia, L. J., ORTEP-3 for windows - a version of ORTEP-III with a graphical user interface (GUI). *J. Appl. Crystallography* **1997,** *30*, 565.

[46] Frisch, M. J.; Trucks, G. W.; Schlegel, H. B.; Scuseria, G. E.; Robb, M. A.; Cheeseman, J. R.; Scalmani, G.; Barone, V.; Mennucci, B.; Petersson, G. A.; Nakatsuji, H.; Caricato, M.; Li, X.; Hratchian, H. P.; Izmaylov, A. F.; Bloino, J.; Zheng, G.; Sonnenberg, J. L.; Hada, M.; Ehara, M.; Toyota, K.; Fukuda, R.; Hasegawa, J.; Ishida, M.; Nakajima, T.; Honda, Y.; Kitao, O.; Nakai, H.; Vreven, T.; Montgomery, J. A., Jr.; Peralta, J. E.; Ogliaro, F.; Bearpark, M.; Heyd, J. J.; Brothers, E.; Kudin, K. N.; Staroverov, V. N.; Kobayashi, R.; Normand, J.; Raghavachari, K.; Rendell, A.; Burant, J. C.; Iyengar, S. S.; Tomasi, J.; Cossi, M.; Rega, N.; Millam, J. M.; Klene, M.; Knox, J. E.; Cross, J. B.; Bakken, V.; Adamo, C.; Jaramillo, J.; Gomperts, R.; Stratmann, R. E.; Yazyev, O.; Austin, A. J.; Cammi, R.; Pomelli, C.; Ochterski, J. W.; Martin, R. L.; Morokuma, K.; Zakrzewski, V. G.; Voth, G. A.; Salvador, P.; Dannenberg, J. J.; Dapprich, S.; Daniels, A. D.; Farkas, Ö.; Foresman, J. B.; Ortiz, J. V.; Cioslowski, J.; Fox, D. J. Gaussian 09, Revision D.01; Gaussian, Inc.: Wallingford, CT, 2009.

[47] Becke, A. D.; Edgecombe, K. E. A simple measure of electron localization in atomic and molecular systems. *J. Chem. Phys.* **1990**, *92,* 5397-5403.

[48] Noury, S.; Krokidis, X.; Fuster, F.; Silvi, B. Computational tools for the electron localization function topological analysis. *Comput. & Chem.***1999**, *23*, 597-604.

[49] Ehlers, A.W.; Böhme, M.; Dapprich, S.; Gobbi, A.; Höllwarth, A.; Jonas, V.; Köhler, K. F.; Stegmann, R.; Veldkamp, A.; Frenking, G. A set of f-polarization functions for pseudo-potential basis sets of the transition metals Sc-Cu, Y-Ag and La-Au. *Chem. Phys. Lett.* **1993**, *208*, 111-114.

[50] Molekel 4.3 from CSCS: http://www.cscs.ch/molekel/

[51] (a) Blanco, M. A.; Martin Pendas, A.; Franscisco E. Interacting Quantum Atoms: A

Correlated Energy Decomposition Scheme Based on the Quantum Theory of Atoms in Molecules *J. Chem. Theory Comput.* **2005**, *1*,1096-1109. (b); Franscisco E.; Martin Pendas, A.; Blanco, M. A. A Molecular Energy Decomposition Scheme for Atoms in Molecules *J. Chem. Theory Comput.* **2006**, *2*, 90-102. (c) Maxwell, P.; Martin Pendas,A.; Popelier, P. L. A. Extension of the interacting quantum atoms (IQA) approach to B3LYP level density functional theory (DFT). *Phys. Chem. Chem. Phys.* **2016**, *18*, 29086-21000.

[52] Keith TA, AIMAll (Version 17.11.14), TK Gristmill Software, Overland Park KS, USA, **2016** (aim.tkgristmill.com).

[53] (a) Cornaton, Y.; Djukic, J.-P. A noncovalent interaction insight onto the concerted metallation deprotonation mechanism. *Phys. Chem. Chem. Phys.* **2019**, *21*, 20486-20498. (b) Pastorczak, E.; Corminboeuf, C. Perspective: Found in translation: Quantum chemical tools for grasping non-covalent interactions. *J. Chem. Phys.* **2017**, *146*, 120901/1-12.

[54] Poater, J.; Duran, M.; Sola, M.; Silvi, B. Theoretical Evaluation of Electron Delocalization in Aromatic Molecules by Means of Atoms in Molecules (AIM) and Electron Localization Function (ELF) Topological Approaches. *Chem. Rev.* **2005**, *105,* 3911-3947.

[55] Silvi, B.; Gillespie, R. J.; Gatti, C. Electron density analysis. *Comprehensive Inorganic Chemistry II* **2013**, *9,* 187-226.

[56] (a) Lepetit, C.; Silvi, B.; Chauvin, R. ELF Analysis of Out-of-Plane Aromaticity and In-Plane Homoaromaticity in Carbo[*N*]annulenes and [*N*]Pericyclynes. *J. Phys. Chem. A* **2003**, *107*, 464-473. (b) Silvi, B. How topological partitions of the electron distributions reveal delocalization. *Phys. Chem. Chem. Phys.* **2004**, *6,* 256-260.

For Table of Contents Only

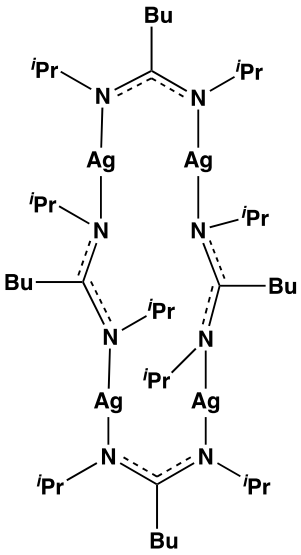

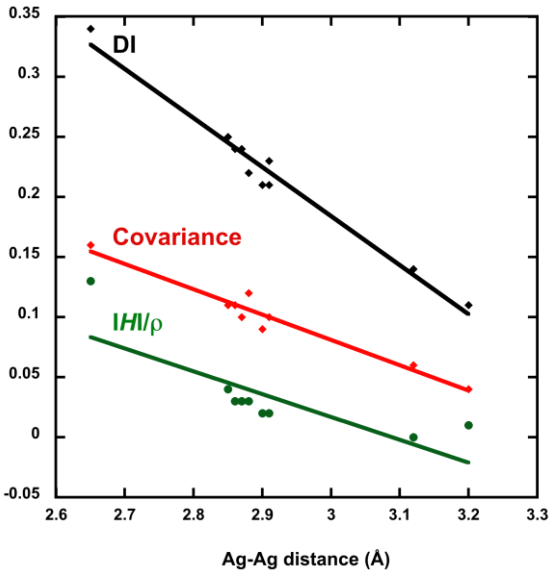

Characterization of the strength and covalence degree
of argentophilic interactions in a series
of four polynuclear silver-amidinates complexes